Available online at www.sciencedirect.com
ScienceDirect
Coastal Engineering 55 (2008) 209–223
Coastal Engineering
An International Journal for Coastal, Harbour and Offshore Engineers
www.elsevier.com/locate/coastaleng

Run-up of tsunamis and long waves in terms of surf-similarity

Per A. Madsen *, David R. Fuhrman

Department of Mechanical Engineering, Technical University of Denmark, 2800 Kgs Lyngby, Denmark

Received 30 April 2007; accepted 5 September 2007
Available online 18 October 2007

Abstract

In this paper we review and re-examine the classical analytical solutions for run-up of periodic long waves on an infinitely long slope as well as on a finite slope attached to a flat bottom. Both cases provide simple expressions for the maximum run-up and the associated flow velocity in terms of the surf-similarity parameter and the amplitude to depth ratio determined at some offshore location. We use the analytical expressions to analyze the impact of tsunamis on beaches and relate the discussion to the recent Indian Ocean tsunami from December 26, 2004. An important conclusion is that extreme run-up combined with extreme flow velocities occurs for surf-similarity parameters of the order 3–6, and for typical tsunami wave periods this requires relatively mild beach slopes. Next, we compare the theoretical solutions to measured run-up of breaking and non-breaking irregular waves on steep impermeable slopes. For the non-breaking waves, the theoretical curves turn out to be superior to state-of-the-art empirical estimates. Finally, we compare the theoretical solutions with numerical results obtained with a high-order Boussinesq-type method, and generally obtain an excellent agreement.

Keywords: Run-up; Tsunamis; Long waves; Surf-similarity

1. Introduction

Within the last couple of years, a large number of publications and reports have addressed the devastating Indian Ocean tsunami event (December 26, 2004). These cover various aspects such as the rupture process (e.g. Ammon et al., 2005; Bilham, 2005), analysis of tide gauges and satellite data (e.g. Borrero, 2005; Gower, 2005; Titov et al., 2005; Geist et al., 2006; Fujii and Satake, 2007), field surveys (e.g. Bagai et al., 2005; Borrero et al., 2006; Harada, 2005) and numerical tsunami modelling (e.g. Titov et al., 2005; Arcas and Titov, 2006; Wang and Liu, 2006; Grilli et al., 2007; Ioualalen et al., 2007). Rather impressive numerical results have been obtained by utilizing detailed rupture information about the deep ocean wave generation and detailed bathymetric maps of the nearshore areas (see e.g. Titov et al., 2005).

In hindsight, many mistakes were actually made in the early aftermath of the tsunami event, when several consulting engineering companies rushed to promote animations of their preliminary numerical simulations of the associated wave motion: The tsunami was typically generated as a ring wave from a single point source (rather than a plane wave generated from a sequence of line sources covering several hundreds of kilometers) and the run-up and flooding of beaches was typically illustrated by breaking 10–20 second wind waves (rather than long waves with periods in the range of 12–50 min). In the press and public media, journalists and engineers tried hard to make popular explanations of the nature of the tsunami monster, but most attempts actually ended up mystifying rather than simplifying the phenomenon. They generally gave the impression that the danger created by a tsunami coming from the deep ocean is due to its gigantic speed (moving as fast as a jet plane) combined with the immense increase in height when it jumps up on the beach.

The fact that tsunamis respond very differently to steep and mild beaches, and that it is the flow velocity during run-up and rundown, which is the crucial parameter for the impact rather than the height itself, has rarely been addressed. In this connection, there is a lesson to be learned e.g. from the Thailand beaches which were exposed to the Indian Ocean tsunami: Flat beaches such as Patong, Kalim, Kamala, Bang Tao and Khao

* Corresponding author.
E-mail address: prm@mek.dtu.dk (P.A. Madsen).

0378-3839/$ - see front matter © 2007 Elsevier B.V. All rights reserved.
doi:10.1016/j.coastaleng.2007.09.007

Lak experienced major destruction, while steeper beaches such as Surin, Karon, Kata, Kata Thani and at the Similan Islands were left almost untouched. Obviously local focusing, refraction, diffraction and reflection may have played an important role and these phenomena are all included in detailed numerical models. It is, however, also possible to explain these observations by means of the analytical solution of Carrier and Greenspan (1958), which has the advantage that it is very simple to use and that it isolates the influence of bed slope and wave period on maximum run-up and velocity. As a first assessment, we consider this approach to be very valuable, and this has inspired the present work.

For completeness, we start with a review of classical solutions by Green (1838), Lamb (1932), Keller and Keller (1964) and Carrier and Greenspan (1958) to the linear and non-linear shallow water equations for periodic long waves on a slope. The linear problem is treated in Section 2, while the non-linear problem is treated in Section 3. In Section 4 we introduce the surf-similarity parameter and the main result is a quantification of the maximum run-up and the associated flow velocity in terms of the surf-similarity parameter and the amplitude to depth ratio determined at some offshore location. In Section 5 we return to a discussion of the Indian Ocean tsunami from December 26, 2004, where measurements off the coastline of Phuket, Thailand provide the necessary information about typical tsunami wave periods and nearshore wave heights. This information is combined with the analytical expressions from Section 5 in an attempt to explain why the tsunami impact on some beaches can be so dramatically worse than on other neighbouring beaches.

In Section 6 we address the problem of run-up of irregular wind waves on steep impermeable slopes. The recent review made by Hughes (2004) has revealed that existing empirical expressions for the run-up of non-breaking regular and irregular waves are quite inadequate to capture the observed scatter. Hughes therefore concludes that the surf-similarity parameter is probably not a good choice as the governing parameter for the run-up. We tend not to agree with this conclusion and successfully apply the Carrier and Greenspan theory to the data of Ahrens (1981).

Finally, in Section 7, we present a numerical model based on a highly accurate Boussinesq-type formulation. This formulation, which was originally derived by Madsen et al. (2002, 2003) for slowly varying bathymetries, has recently been extended to allow rapidly varying bathymetries (see Madsen et al., 2006) as well as to moving wet/dry shorelines (see Fuhrman and Madsen, in press). Although the formulation allows for dispersive non-linear wave motion, we concentrate on the run-up of long waves and compare the computations with the analytical expressions presented in Sections 2–4.

2. Linear solution to the run-up of periodic long waves

Tsunamis usually have relatively long wave periods, and it is generally a good approximation to assume hydrostatic pressure and a uniform vertical distribution of the velocity field. This means that under most circumstances tsunamis can be modelled by the non-linear shallow water equations. Throughout this work, we deal with one-dimensional motion only i.e. waves perpendicular to the shoreline. Furthermore, as a first assessment, we linearize the non-linear shallow water equations and consider

$$\frac{\partial \eta}{\partial t}+\frac{\partial}{\partial x}(hU)=0, \qquad \frac{\partial U}{\partial t}+g\frac{\partial \eta}{\partial x}=0, \tag{1}$$

where η is the surface elevation, h the still water depth, g the acceleration of gravity and U the velocity components in the x direction. These two first-order equations can be transformed into the second order equation

$$\frac{\partial^2 \eta}{\partial t^2}-g\frac{\partial}{\partial x}\left(h\frac{\partial \eta}{\partial x}\right)=0. \tag{2}$$

by cross-differentiation and elimination of U. We focus on analytical run-up solutions, which can be obtained under the following assumptions: 1) the beach slope γ is constant; 2) the effects of wave breaking and bottom dissipation can be neglected; 3) full reflection occurs from the shoreline; 4) the wave motion is linear and periodic. In the following, we review and discuss the linear solutions previously derived by Green (1838), Lamb (1932) and Keller and Keller (1964).

2.1. The linear far-field solution on a constant slope

A first description of waves approaching a sloping beach can be obtained by using the classical WKBJ expansion assuming a mild beach slope. Green (1838) derived this solution in his work on the motion of waves in a variable canal of small depth and width, see also Lamb (1932, §185). We consider a slowly varying bathymetry $h(\delta x)$, where δ is an ordering parameter, with the x-axis starting at the shoreline and pointing towards the sea. A linear wave propagating towards the shore can now be described by

$$\eta(x,t)=A(\delta x)\ \cos\left(\omega t+\int k(\delta x)\mathrm{d}x\right), \tag{3}$$

where ω is the cyclic frequency, $k(\delta x)$ is the wave number and $A(\delta x)$ the wave amplitude, both slowly varying in space. We insert (3) into (2) and collect terms in powers of δ. The zeroth order problem now yields the dispersion relation

$$k=\frac{\omega}{\sqrt{gh}}, \tag{4}$$

while the first-order problem yields the linear shoaling equation

$$\frac{1}{h}\frac{\mathrm{d}h}{\mathrm{d}x}+\frac{1}{k}\frac{\mathrm{d}k}{\mathrm{d}x}+\frac{2}{A}\frac{\mathrm{d}A}{\mathrm{d}x}=0. \tag{5}$$

We differentiate (4) with respect to x, insert this result in (5), and integrate the equation to obtain

$$A(x)=A_0\left(\frac{h(x)}{h_0}\right)^{-1/4} \tag{6}$$

where A_0 denotes the incoming wave amplitude at depth h_0. This is the classical shoaling law of Green (1838). Utilizing that the beach slope γ is constant i.e. $h(x)=\gamma x$, we obtain

$$k=\frac{\omega}{\sqrt{g\gamma x}} \quad \Rightarrow \int k\mathrm{d}x = 2\omega\sqrt{\frac{x}{g\gamma}}. \tag{7}$$

Hence, according to (3), (6) and (7) the incoming wave can be expressed by

$$\eta(x,t)=A_0\left(\frac{\gamma x}{h_0}\right)^{-1/4}\cos\left(\omega t+2\omega\sqrt{\frac{x}{g\gamma}}\right). \tag{8}$$

We emphasize that the linear approach, cannot predict a moving shoreline (in contrast to the non-linear approach presented in Section 3). Hence the shoreline is fixed at $x=0$, and we notice that (8) is strictly not valid here, as the amplitude goes to infinity for $x\to 0$. Nevertheless, we assume that the incoming wave is fully reflected from the shore and add an equivalent outgoing wave, to obtain the standing wave solution

$$\eta(x,t)=2A_0\left(\frac{\gamma x}{h_0}\right)^{-1/4}\cos\left(2\omega\sqrt{\frac{x}{g\gamma}}+\varphi\right)\cos\,\omega t \text{ for } x>0. \tag{9}$$

Here φ denotes an unknown phase shift, which will be determined in the following.

2.2. The linear near-field solution on a constant slope

Lamb (1932, §186), presented a linear long wave solution, which is also valid in the vicinity of the shoreline. Again, a constant beach slope is assumed i.e. $h(x)=\gamma x$, but the previous assumption of a mildly sloping beach is relaxed, and we now look for solutions of the form

$$\eta(x,t)=A(x)\cos\,\omega t, \quad U(x,t)=B(x)\sin\,\omega t. \tag{10}$$

By inserting (10) into (2) and (1) we obtain

$$x\frac{d^2A}{\mathrm{d}x^2}+\frac{\mathrm{d}A}{\mathrm{d}x}+\frac{\omega^2}{g\gamma}A=0, \quad B=-\frac{g}{\omega}\frac{\mathrm{d}A}{\mathrm{d}x}. \tag{11}$$

Next, inspired by (7), we introduce the coordinate transformation

$$\sigma\equiv 2\omega\sqrt{\frac{x}{g\gamma}}, \tag{12}$$

by which (11) simplifies to

$$\frac{\mathrm{d}^2A}{\mathrm{d}\sigma^2}+\frac{1}{\sigma}\frac{\mathrm{d}A}{\mathrm{d}\sigma}+A=0, \quad B=-\frac{2\omega}{\sigma\gamma}\frac{\mathrm{d}A}{\mathrm{d}\sigma}. \tag{13}$$

This is the Bessel equation of the first kind, and the solution to this equation can be expressed by

$$A(\sigma)=RJ_0(\sigma), \quad B(\sigma)=\frac{2\omega R}{\sigma\gamma}J_1(\sigma), \tag{14}$$

where J_n is the nth order Bessel function of the first kind and R is an unknown amplitude. Consequently, the near-field solutions for the surface elevation and the flow velocity become

$$\eta(x,t)=RJ_0(\sigma)\cos\,\omega t, \quad U(x,t)=\frac{2\omega R}{\sigma\gamma}J_1(\sigma)\sin\,\omega t. \tag{15}$$

Approaching the fixed shoreline ($\sigma\to 0$) leads to $J_0(\sigma)\to 1$ and $J_1(\sigma)\to\sigma/2$ by which we obtain

$$\eta\to R\cos\,\omega t \text{ for } \sigma\to 0, \quad U\to\frac{\omega R}{\gamma}\sin\,\omega t \text{ for } \sigma\to 0. \tag{16}$$

In order to determine the run-up elevation R and the associated flow velocity $V=\omega R/\gamma$ for a given incoming wave, it is necessary to match the near-field and far-field solutions. For this purpose, we utilize the asymptotic approximations to the Bessel functions for large arguments (see e.g. Bowman, 1958)

$$J_0(\sigma)\to\sqrt{\frac{2}{\pi}}\sigma^{-1/2}\cos\left(\sigma-\frac{\pi}{4}\right), \quad \text{for } \sigma\gg 1, \tag{17}$$

$$J_1(\sigma)\to\sqrt{\frac{2}{\pi}}\sigma^{-1/2}\sin\left(\sigma-\frac{\pi}{4}\right), \quad \text{for } \sigma\gg 1, \tag{18}$$

in which case (15) simplifies to

$$\eta(x,t)\to\frac{R}{\sqrt{\pi\omega}}\left(\frac{x}{g\gamma}\right)^{-1/4}\cos\left(2\omega\sqrt{\frac{x}{g\gamma}}-\frac{\pi}{4}\right)\cos\,\omega t, \tag{19}$$

$$U(x,t)\to\frac{\omega R}{\gamma\sqrt{\pi\omega}}\left(\frac{x}{g\gamma}\right)^{-1/4}\sin\left(2\omega\sqrt{\frac{x}{g\gamma}}-\frac{\pi}{4}\right)\sin\,\omega t, \tag{20}$$

for $\sigma\gg 1$.

We match (19) and the linear shallow water far-field solution (9), by which we obtain

$$\frac{R}{A_0}=2\sqrt{\pi}\left(\frac{h_0\omega^2}{g\gamma^2}\right)^{1/4}, \quad V=\frac{\omega R}{\gamma}. \tag{21}$$

This defines the maximum run-up and the associated flow velocity for given shallow water far-field conditions h_0, A_0 and ω and for a given bed slope γ.

2.3. A constant slope connected to a flat offshore region

So far, we have considered the run-up on a constant and infinitely long slope. A more common problem, however, is a finite slope connected to an offshore constant-depth region. Keller and Keller (1964) studied this problem by assuming linear wave motion in both regions and by matching the solutions at the toe of the slope. In the following we briefly review their solution.

Again the x-axis starts at the initial shoreline and points towards the sea with a depth variation defined by

$$h(x)=\gamma x, \quad x\le x_0,$$
$$h(x)=h_0, \quad x\ge x_0.$$

The toe of the slope is located at x_0, the depth of the flat region is $h_0=\gamma x_0$ and in this region the wave number of the incoming shallow water wave is given by

$$k_0=\frac{\omega}{\sqrt{gh_0}}. \tag{22}$$

The incoming and the reflected wave solutions in the constant-depth region are given by

$$\eta_i(x,t)=A_0e^{-i(\omega t+k_0x)},\quad \eta_r(x,t)=A_re^{-i(\omega t-k_0x)}, \tag{23}$$

where i is the imaginary unit, A_0 is the incoming wave amplitude (a real number) and A_r is the amplitude of the reflected wave (a complex number). In agreement with (15), the linear standing wave solution on the sloping beach is described by

$$\eta_s(x,t)=A_sJ_0(\sigma)e^{-i\omega t}, \tag{24}$$

where σ is defined by (12), A_s is the run-up amplitude (a complex number) and J_0 the zeroth order Bessel function of the first kind. At the toe of the slope we match the surface elevations and particle velocities from the two regions. According to (1) this is equivalent to the conditions

$$\eta_i+\eta_r=\eta_s \quad \text{for } x=x_0, \tag{25}$$

$$\frac{\partial\eta_i}{\partial x}+\frac{\partial\eta_r}{\partial x}=\frac{\partial\eta_s}{\partial x} \quad \text{for } x=x_0. \tag{26}$$

By inserting (23)–(24) into (25)–(26), we can determine A_r and A_s and in combination with (24) this leads to the solution

$$\eta_s(x,t)=\left(\frac{2J_0(\sigma)}{J_0(\sigma_0)-iJ_1(\sigma_0)}\right)\eta_i(x_0,t), \tag{27}$$

where

$$\sigma_0\equiv 2\omega\sqrt{\frac{x_0}{g\gamma}}=2\sqrt{\frac{h_0\omega^2}{g\gamma^2}}. \tag{28}$$

As a result, the run-up elevation becomes

$$\frac{R}{A_0}=\left|\frac{2}{J_0(\sigma_0)-iJ_1(\sigma_0)}\right|. \tag{29}$$

Intuitively, one would expect this solution to be similar to (21) provided that the finite sloping beach covers a sufficiently large fraction of the incoming wave length. In fact, the physical interpretation of the parameter σ_0 can be related to this fraction by using that

$$L_0=T\sqrt{gh_0}=2\pi\sqrt{\frac{gh_0}{\omega^2}},$$

and according to (28) we get the relation

$$\sigma_0=4\pi\left(\frac{x_0}{L_0}\right). \tag{30}$$

If $\sigma_0\gg 1$, we can again utilize the asymptotic approximations to the Bessel functions for large arguments i.e. (17)–(18), which leads to

$$\left(\frac{1}{J_0(\sigma_0)-iJ_1(\sigma_0)}\right)\rightarrow\sqrt{\frac{\pi}{2}}\sqrt{\sigma_0}e^{i(\sigma_0-\pi/4)},\quad \text{for } \sigma_0>>1. \tag{31}$$

In this case (29) simplifies to

$$\frac{R}{A_0}=\sqrt{2\pi\sigma_0}=2\sqrt{\pi}\left(\frac{h_0\omega^2}{g\gamma^2}\right)^{1/4}. \tag{32}$$

This is identical to (21) obtained for an infinitely long slope.

Another approximation to (29) can be obtained by utilizing (17) for J_0 but replacing (18) by

$$J_1(\sigma_0)\rightarrow\sqrt{\frac{2}{\pi}}\sigma_0^{-1/2}\sin\left(\sigma_0-\frac{\pi}{4}\right)+\frac{1}{\sqrt{2\pi}}\sigma_0^{-3/2}\cos\left(\sigma_0-\frac{\pi}{4}\right),\quad \text{for } \sigma>>1, \tag{33}$$

which corresponds to a direct differentiation of (17) with respect to σ. This leads to the solution

$$\frac{R}{A_0}=\sqrt{2\pi}\left|\frac{\sigma_0^{3/2}}{(1+2i\sigma_0)\cos(\sigma_0-\pi/4)+2\sigma_0\sin(\sigma_0-\pi/4)}\right|. \tag{34}$$

Fig. 1 shows the variation of (29), (32), and (34) as a function of σ_0. We notice that (34) is a good approximation to (29) for $\sigma_0\geq\pi/2$ i.e. for $x_0/L_0>1/8$. On the other hand, discrepancies between (29) and (32) remain for much larger values of σ_0, and although the importance of the second term in (33) decreases for increasing values of σ_0, this term retains the oscillating nature of the response. Fig. 2 shows the ratio between (a) (32) and (29), and (b) (34) and (29). While the latter is converging towards unity quite rapidly, the former has a very slow convergence.

3. Non-linear solution to the run-up of periodic long waves

In the previous section, run-up solutions were obtained by assuming linear shallow water theory everywhere. While this is

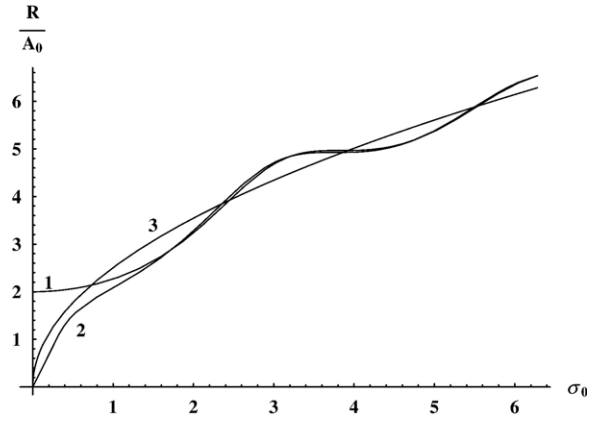

Fig. 1. The run-up as a function of σ_0. 1: Finite slope solution (29); 2: approximate finite slope solution (34); 3: infinite slope solution (32).

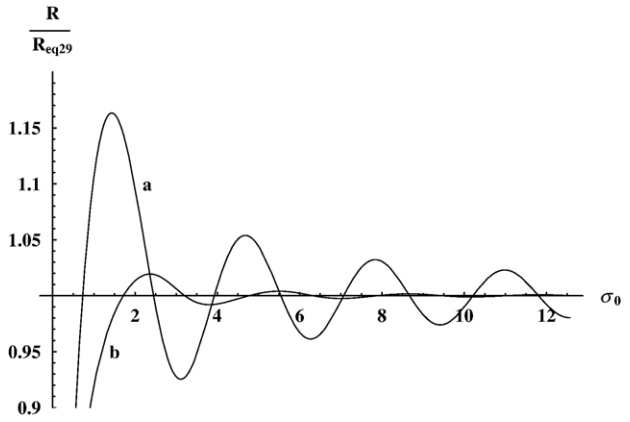

Fig. 2. Run-up ratios as a function of σ_0. a: Ratio between (32) and (29); b: ratio between (34) and (29).

typically a good approximation in the far-field, where the waves propagate in the deep ocean, it is obvious that non-linearity plays an important role during the shoaling and run-up process. To deal with this problem we now consider solutions to the non-linear shallow water equations

$$\frac{\partial \eta}{\partial t}+\frac{\partial}{\partial x}(U(h+\eta))=0, \quad \frac{\partial U}{\partial t}+U\frac{\partial U}{\partial x}+g\frac{\partial \eta}{\partial x}=0. \tag{35}$$

It is not a trivial task to obtain analytical solutions to these equations, but Carrier and Greenspan (1958) provided an elegant method in their pioneering work, and we shall summarize this method in the following.

3.1. The non-linear solution on a constant slope

Various formulations of Carrier and Greenspan's method can be found in e.g. Gjevik and Pedersen (1981), Synolakis (1987), Mei (1989) and Carrier et al. (2003). Here we first transform the independent coordinates from (x, t) to

$$\lambda \equiv -\frac{1}{2g\gamma}(\alpha+\beta), \quad \rho \equiv \frac{1}{2g\gamma}(\alpha-\beta), \tag{36}$$

where C is the wave celerity and (α, β) the Riemann invariants defined by

$$\alpha \equiv U+2C-g\gamma t, \quad \beta \equiv U-2C-g\gamma t, \quad C \equiv \sqrt{g(h+\eta)}. \tag{37}$$

Hence (36) and (37) leads to

$$\lambda = t-\frac{U}{g\gamma}, \quad \rho=\frac{2C}{g\gamma}. \tag{38}$$

Second, we introduce the dependent variable $\psi(\rho, \lambda)$ defined by

$$\frac{\partial \psi}{\partial \rho}=\rho U, \quad \frac{\partial \psi}{\partial \lambda}=2\left(x-\frac{U^2}{2g\gamma}-\frac{g\gamma\rho^2}{4}\right). \tag{39}$$

By following the procedure outlined e.g. in Mei (1989), the two original non-linear equations in η and U can now be simplified to a single linear equation in ψ,

$$\frac{\partial}{\partial \rho}\left(\rho\frac{\partial \psi}{\partial \rho}\right)-\rho\frac{\partial^2 \psi}{\partial \lambda^2}=0. \tag{40}$$

This is the main achievement of using Carrier and Greenspan's technique. The remaining step is to determine η, U, x and t in terms of ψ, ρ and λ. From (37)–(39) we obtain

$$t(\rho,\lambda)=\lambda+\frac{U}{g\gamma}, \tag{41}$$

$$x(\rho,\lambda)=\frac{1}{2}\frac{\partial \psi}{\partial \lambda}+\frac{U^2}{2g\gamma}+\frac{g\gamma\rho^2}{4}, \tag{42}$$

$$\eta(\rho,\lambda)=\left(\frac{g\gamma^2\rho^2}{4}-\gamma x\right)=-\left(\frac{\gamma}{2}\frac{\partial \psi}{\partial \lambda}+\frac{U^2}{2g}\right), \tag{43}$$

$$U(\rho,\lambda)=\frac{1}{\rho}\frac{\partial \psi}{\partial \rho}, \tag{44}$$

which define the non-linear solution as a set of parametric curves in terms of ρ and λ.

The moving shoreline is defined by $h+\eta=0$, i.e. $\eta=-\gamma x$ and according to (43) this is achieved for $\rho=0$. A periodic solution to (40), which is finite for $\rho=0$ reads

$$\psi(\rho,\lambda)=-\frac{2R}{\gamma\omega}J_0(\omega\rho)\ \sin\ (\omega\lambda), \tag{45}$$

where J_0 is the zeroth order Bessel function of the first kind and R is an unknown amplitude. By inserting (45) into (43) and (44) we get

$$U(\rho,\lambda)=\frac{2R}{\gamma\rho}J_1(\omega\rho)\ \sin\ (\omega\lambda), \tag{46a}$$

$$\eta(\rho,\lambda)=RJ_0(\omega\rho)\ \cos\ (\omega\lambda)-\frac{U^2}{2g}. \tag{46b}$$

In order to determine R for a given incoming wave, it is necessary to match the near-field and far-field solutions. Far away from the shoreline, we assume that wave conditions can be linearized and obtain

$$\omega\rho=\frac{2\omega}{g\gamma}\sqrt{g(h+\eta)} \ \rightarrow\ 2\omega\sqrt{\frac{x}{g\gamma}}=\sigma, \tag{47}$$

$$\omega\lambda=\omega\left(t-\frac{U}{g\gamma}\right) \ \rightarrow\ \omega t. \tag{48}$$

This indicates that ρ represents the spatial coordinate, while λ represents the temporal coordinate. Furthermore, the expressions in (46) linearize to

$$U(x,t)\rightarrow\frac{2\omega R}{\gamma\sigma}J_1(\sigma)\ \sin\ \omega t, \quad \eta(x,t)\rightarrow RJ_0(\sigma)\ \cos\ \omega t. \tag{49}$$

This is seen to be in perfect agreement with the linear result (15). Hence, if we again utilize the asymptotic approximations to the Bessel functions for large arguments i.e. (17)–(18) and match the results with the linear far-field solution (9), we obtain

$$\frac{R}{A_0} = 2\sqrt{\pi}\left(\frac{h_0\omega^2}{g\gamma^2}\right)^{1/4}, \tag{50}$$

in agreement with the linear result (21).

We can now determine the non-linear shoreline solution by letting $\rho \to 0$ in (46), which yields

$$U(0,\lambda) = -\frac{\omega R}{\gamma}\,\sin\,(\omega\lambda), \tag{51a}$$

$$\eta(0,\lambda) = R\left(\cos\,(\omega\lambda) - \frac{R\omega^2}{2g\gamma^2}\,\sin^{\,2}(\omega\lambda)\right). \tag{51b}$$

For $R \le g\gamma^2/\omega^2$ (a condition which will be discussed in the next section), the maximum run-up and drawn-down elevations will be $\pm R$, while the maximum velocities will be $V = \pm\omega R/\gamma$. Hence it turns out that the non-linear solution for maximum run-up/draw-down elevations and velocities are identical to the linear results given in (21). This surprising result was first emphasized by Synolakis (1987). On the other hand, in contrast to the linear solution, which has a fixed shoreline at $x=0$, the non-linear solution has a moving shoreline, where x varies between $-R/\gamma$ and R/γ. Because of this, the spatial and temporal variations of η and U will actually deviate significantly from the linear solution close to the shoreline.

3.2. A theoretical breaking criterion

While ψ given by (45) is always a single-valued function of ρ and λ, it may become multi-valued in terms of x and t, and if this happens the mapping between (x, t) and (ρ, λ) formally breaks down. This mapping is governed by the Jacobian

$$J = \frac{\partial(x,t)}{\partial(\rho,\lambda)} = \frac{\partial x}{\partial\rho}\frac{\partial t}{\partial\lambda} - \frac{\partial x}{\partial\lambda}\frac{\partial t}{\partial\rho}, \tag{52}$$

and we can easily determine the ρ and λ derivatives of x and t by the use of (42) and (41) combined with (44) and (45). Since it is expected that the transformation becomes singular close to the shoreline, we expand the resulting Jacobian for $\rho \to 0$ and obtain

$$J \to -\frac{\rho}{16g^2\gamma^2}\left(1 + \frac{R\omega^2}{g\gamma^2}\,\cos\,(\omega\lambda)\right)^2 + O(\rho^2), \quad \text{for } \rho \to 0.$$

Consequently, the break-down criterion reads

$$R \le R_{\text{break}} = \frac{g\gamma^2}{\omega^2}. \tag{53}$$

This criterion corresponds to a vertical surface elevation during draw-down, and as such it could be interpreted as an indication of physical wave breaking. Mei et al. (2005) argue that (53) is meaningful only as a qualitative rather than a quantitative measure of wave breaking, and that R should not be too close to this limiting value for the solution to be valid. Synolakis (1987), on the other hand, argues that in general the shallow water wave formalism predicts wave breaking earlier than it actually happens in nature. His conclusion is supported by experimental data for breaking and non-breaking solitary waves. We tend to agree with Synolakis, and this conclusion will be supported by measurements of irregular wave run-up on smooth impermeable structures in Section 6.

4. Maximum run-up in terms of the surf-similarity parameter

Waves on beaches and their type of breaking depend on the beach slope, the wave period and a representative wave height (either offshore or nearshore). Iribarren and Nogales (1949), Galvin (1968) and Battjes (1974) characterized the beach processes in terms of the non-dimensional surf-similarity parameter (also known as the Iribarren number) defined by

$$\xi_\infty \equiv \frac{\gamma}{\sqrt{H_\infty/L_\infty}}, \tag{54}$$

where H_∞ is the deep-water wave height and L_∞ is the linear deep-water wave length. In terms of this parameter, Galvin (1968) classified the breaker types on plane impermeable beaches by

$$\begin{aligned} \xi_\infty < 0.5 \quad &\Rightarrow \quad \text{spilling},\\ 0.5 < \xi_\infty < 3.3 \quad &\Rightarrow \quad \text{plunging},\\ 3.3 < \xi_\infty \quad &\Rightarrow \quad \text{surging}. \end{aligned}$$

Because of their relatively short wave periods (and wave lengths) wind waves will typically have rather small ξ_∞ on most beaches (leading to spilling or plunging breaking), while tsunamis will have rather large values (leading to surging and full reflection). Not surprisingly, the surf-similarity parameter also plays an important role for the run-up of breaking and non-breaking wind waves on beaches and steep structures. Hughes (2004) concluded that most empirical run-up expressions are given in terms of ξ defined by

$$\xi \equiv \frac{\gamma}{\sqrt{H_0/L_\infty}}, \tag{55}$$

where H_0 is the local wave height at or near the toe of the slope.

While the surf-similarity parameter undoubtedly has been a successful tool in the classification of breaking and run-up of wind waves, it is rarely used to characterize the impact of tsunamis on beaches. One reason could be that a tsunami is not really a periodic phenomenon but rather a transient phenomenon of limited duration. However, if we accept the assumption of the tsunami being a quasi-periodic phenomenon (a case which is certainly supported by some observations, see e.g. Fig. 5), we obtain the maximum run-up solutions (29), (32) and

(34). These can very easily be expressed in terms of the surf-similarity parameter, by using that

$$\sigma_0 = 2\sqrt{\frac{h_0\omega^2}{g\gamma^2}} = 2\sqrt{\pi}\xi^{-1}\left(\frac{A_0}{h_0}\right)^{-1/2}. \tag{56}$$

As an example, (32) can be expressed as

$$\frac{R}{A_0} = 2\pi^{3/4}\left(\frac{A_0}{h_0}\right)^{-1/4}\xi^{-1/2}. \tag{57}$$

Similarly, the associated maximum flow velocity, which is determined by $V=\omega R/\gamma$, can be expressed as

$$\frac{V}{\sqrt{gA_0}} = \frac{\sqrt{\pi}}{\xi}\left(\frac{R}{A_0}\right). \tag{58}$$

Finally, the theoretical breaking criterion (53) can be expressed as

$$\frac{R_{\text{break}}}{A_0} = \frac{1}{\pi}\xi^2. \tag{59}$$

Notice that R from (57) and R_{break} from (59) represent two different sets of curves, which intersect at the theoretical break point ξ_{break}. Generally, the run-up increases with decreasing values of ξ as long as $\xi \geq \xi_{\text{break}}$. For $\xi < \xi_{\text{break}}$ we may, as a first approximation, assume that R will follow R_{break}, which corresponds to a saturated model of wave breaking. With this assumption, which will be tested in Section 6, we combine the two sets of curves by determining $R^* = \min(R, R_{\text{break}})$. Fig. 3 shows a comparison between (57) as dashed lines and (29) as full lines. In general there is little difference between the two solutions. We notice, that the smaller the A_0/h_0, the larger the amplification R/A_0 can become before breaking takes over. As tsunamis typically initiate as very small waves on large water depths, the ratio A_0/h_0 can easily be as small as say 0.001 or less. The largest run-up will typically occur if ξ falls in the interval $3 \lesssim \xi \lesssim 6$, where the transition from non-breaking to breaking waves occurs. Fig. 4 shows the associated maximum flow velocity near the shoreline determined by (58). Again we notice, that the smaller the A_0/h_0 ratio the larger the maximum velocity $V/\sqrt{gA_0}$. These results will be utilized in Section 5 to discuss the impact of tsunamis on beaches.

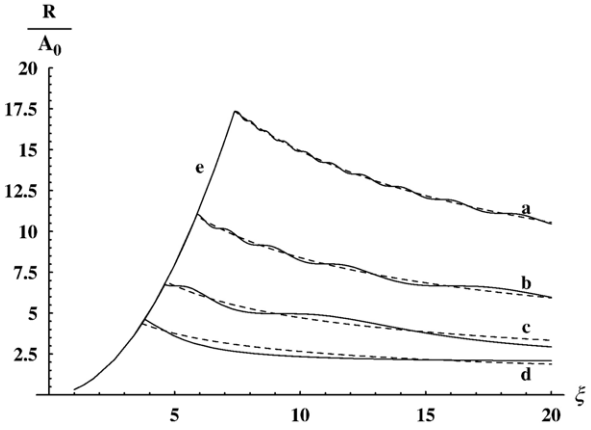

Fig. 3. The non-dimensional run-up elevation as a function of the surf-similarity parameter ξ. Dashed lines: Infinite slope solution i.e. (57). Full lines: The finite slope solutions i.e. (29) with (56). a: $A_0/h_0=0.0001$; b: $A_0/h_0=0.001$; c: $A_0/h_0=0.01$; d: $A_0/h_0=0.1$. e: Theoretical breaking criterium $R/A_0=\xi^2/\pi$.

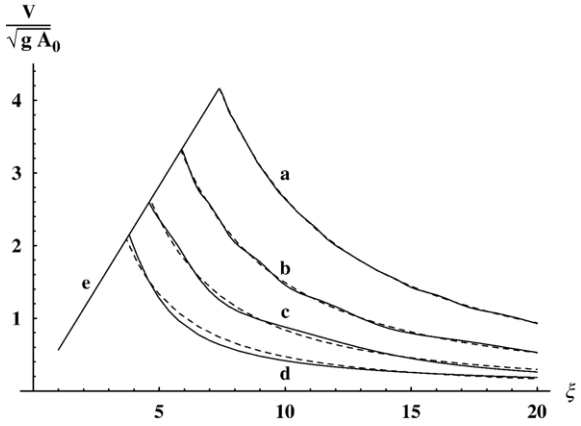

Fig. 4. The non-dimensional maximum run-up velocity as a function of the surf-similarity parameter ξ. Dashed lines: Infinite slope solution i.e. (58) with (57). Full lines: The finite slope solutions i.e. (58) with (29) and (56). a: $A_0/h_0=0.0001$; b: $A_0/h_0=0.001$; c: $A_0/h_0=0.01$; d: $A_0/h_0=0.1$. e: Theoretical breaking criterium $R/A_0=\xi^2/\pi$.

5. Relevance to observed tsunami impact on beaches

The impact of waves on shorelines turns out to be a critical balance between the steepness of the beach and the wave length (or wave period). On one hand, wind waves are generally quite short and they will experience substantial breaking on mild as well as on steep beaches, which dissipates most of their energy before they reach the shoreline. Hence, run-up elevations as well as flow velocities generated by wind waves will be minor. Tides, on the other hand, are extremely long, and from their point of view even the mildest beach acts like a vertical wall. Hence, although tides may result in significant run-up elevations, the associated beach velocities are almost nil. As an example, let us consider a tidal wave with period $T=12$ h and amplitude $A_0=5$ m in $h_0=100$ m i.e. $A_0/h_0=0.05$. On a mild slope of $\gamma=1/120$ this leads to $\xi=142$, $R=4.2$ m and $V=0.07$ m/s i.e. an extremely small flow velocity. An exception is the formation of tidal bores, which occur if extreme tides are further amplified by special bathymetric conditions such as rapidly decreasing cross-sections and water depths. As an example, the Huangzhou bore south of Shanghai in China, can move with a speed of up to 40 km/h, with a steep front where the surface level jumps 3–5 m within 5 min, and with the maximum flow velocities exceeding 5–6 m/s (see e.g. Madsen et al., 2005). However, such extreme tidal events cannot happen at random on beaches, but will occur only in funnel shaped bays and attached rivers.

It is the combination of huge run-up elevations and extreme run-up velocities which makes the tsunami such a unique and

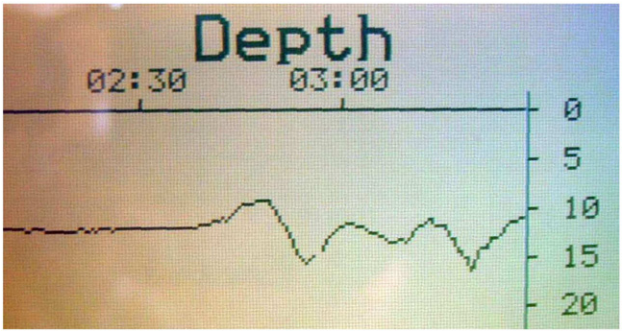

Fig. 5. Sound-meter registration of the Indian Ocean tsunami on December 26, 2004 from the yacht Mercator in the bay of Nai Harn, at the southwestern tip of Phuket, Thailand. Vertical axis measures depth in meters (from the keel i.e. 2 m below mean water level); Horizontal axis measures time in hours. Source: Thomas Siffer (www.thomassiffer.be).

devastating event. The maximum impact will occur whenever the breaking criterion (59) is close to being satisfied i.e. for ξ in the range of 3 to 6. For typical tsunami periods of 2 min $\leq T \leq$ 30 min, it turns out that the beach slope is a very critical parameter in the determination of the tsunami impact. As one example let us consider a wave with period $T=13$ min, and with the amplitude of $A_0=0.75$ m in a depth $h_0=2000$ m, i.e. $A_0/h_0=0.000375$. On a steep slope of $\gamma=1/15$ this leads to $\xi=53$, $R=3.5$ m and $V=0.42$ m/s, i.e. quite a moderate impact on the shoreline. In contrast, on a slope of $\gamma=1/120$ the same tsunami leads to $\xi=6.6$, $R=9.9$ m and $V=9.5$ m/s. In this case the impact is devastating with forces (proportional to V^2) more than 500 times higher! As another example let us again consider a period of $T=13$ min, but now with a wave amplitude of $A_0=2.5$ m in $h_0=14$ m. On a steep slope of $\gamma=1/15$ this leads to $\xi=29$, $R=3.4$ m and $V=0.4$ m/s. In contrast, on a slope of $\gamma=1/120$ the same tsunami leads to $\xi=3.6$, $R=9.5$ m and $V=9.2$ m/s, i.e. again a devastating impact with a factor 530 on the associated forces.

In fact, these two examples are both inspired by observations from the recent Indian Ocean tsunami from December 26, 2004. On this occasion Thomas Siffer from Belgium had anchored his yacht Mercator near the bay of Nai Harn, at the southwestern tip of Phuket, Thailand. During the passage of the tsunami, Mercator's fish-finder (sound-meter) made the recording shown in Fig. 5, where the vertical axis shows the depth in meters, while the horizontal axis shows the time in hours. When reading the depth off the figure, you should add 2.1 m to compensate for the depth of the keel. Note that the average depth at the location is 14 m, and that the initial disturbance is a wave trough of −2.7 m followed by a wave crest of +3.9 m i.e. a wave height of 6.6 m. The second trough is only −0.5 m followed by a crest of +1.7 m, while the third trough is −0.6 m followed by a crest of +4.9 m. Beyond the first crest, the signal is likely influenced by reflections from the nearby coastline. Although the crest and trough heights vary over time, the timespan between successive crests or troughs is approximately 13–14 min during the registration. Hence, although the event is basically a transient phenomenon, we may approximate it by a regular wave event with a period of 13–14 min and with an average wave amplitude of $A_0=2.5$ m in the depth of $h_0=14$ m. In general, wave periods associated with the Indian Ocean tsunami were scattered in the range from 12–50 min as shown by wavelet analysis of tide gauges at the Maldives (se e.g. Titov et al., 2005).

It is a fact that some beaches in Thailand were severely damaged while other nearby beaches were almost untouched. Obviously, local refraction/diffraction effects played an important role, but a very important factor was undoubtedly the local beach slope. The following observations from Thailand were

Fig. 6. A map of a selected region of Thailand affected by the Indian Ocean tsunami on December 26, 2004. The arrow indicates the incoming tsunami direction.

made by Rex Towers from BBC Guernsey (see the map in Fig. 6):

> Just two miles round the headland north of Kalim is Kamala Bay. There is awful devastation there. With hardly any rise in the seabed approaching the land there was nothing to cushion the wall of water coming onto the land. The coastline is flat too, going inland for nearly a mile, so the water went that far in places. Just a mile round the headland from Kamala is Surin beach, and what a difference here. It's like nothing ever happened, and very little did. The steep incline of the beach took the force out of the wall of water and only a few feet came up under the treeline, moving beach chairs and restaurant furniture about.

While unscientific, these observations agree remarkably well with the simple calculations made above on the basis of (57), (58) and (59).

6. Maximum run-up of wind waves on smooth impermeable steep slopes

This section serves two purposes: First, we demonstrate that the derived run-up expressions can be applied not only to tsunamis but also to predict the run-up of non-breaking irregular wind waves on steep slopes. Second, a comparison with experimental data for breaking waves will test the theoretical limiting criterion derived from the non-linear shallow water equations.

Hughes (2004) recently re-examined wave run-up data for regular, irregular and solitary waves on smooth impermeable plane slopes. The goal of his study was to provide a new estimation technique that was as good as existing formulas for breaking waves but better at estimating the run-up of non-breaking waves. For regular waves he compared the empirical relation established by Hunt (1959)

$$\frac{R}{H_0} = \xi, \quad \text{for } \xi \le 3, \tag{60}$$

$$\frac{R}{H_0} = 3.0, \quad \text{for } \xi > 3, \tag{61}$$

with measurements by Granthem (1953) and Saville (1956). He concluded that the breaking waves followed (60) quite closely, while the non-breaking waves were severely scattered and significantly lower than predicted by (61). For irregular waves Burcharth and Hughes (2002) considered the data set produced by Ahrens (1981) for steep slopes ranging from $0.25 \le \gamma \le 1.0$. In this connection empirical relations were established for the ratio $R_{0.02}/H_{m0}$, where $R_{0.02}$ is the vertical elevation from the still water level exceeded by 2% of the run-ups, and H_{m0} is the zeroth-moment of the energy spectrum at the foot of the slope. Assuming a Rayleigh distribution $R_{0.02}$ was estimated to be $1.6R_s$, where R_s is the significant wave run-up, and consequently a direct generalization of (60)–(61) would be to simply multiply the regular wave formula by a factor 1.6. Instead they slightly modified Hunt's (1959) formula to

$$\frac{R_{0.02}}{H_{m0}} = 1.6\xi \quad \text{for } \xi \le 2.5, \tag{62}$$

$$\frac{R_{0.02}}{H_{m0}} = 4.5 - 0.2\xi \quad \text{for } 2.5 \le \xi \le 9, \tag{63}$$

so that for non-breaking waves the constant was replaced by a decreasing trend for increasing ξ. They found that the experimental data supported the breaking curve (for $\xi \le 2.5$) rather closely, while a significant scatter showed up in the non-breaking regime.

Hughes (2004) concluded that run-up data for non-breaking waves that surge up steeper slopes does not correlate very well to ξ, and that *instead* the run-up appears to be directly related to the wave height and the water depth at the toe of the structure. Consequently, Hughes proposed an alternative run-up formula of the form

$$\frac{R}{h_0} \sim \gamma \sqrt{\frac{M_F}{\rho g h_0^2}},$$

where M_F is the maximum wave momentum flux at the toe of the slope. For linear shallow water waves, this simplifies to $M_F = \rho g h_0 A_0$, which leads to

$$\frac{R}{h_0} \sim \gamma \left(\frac{A_0}{h_0}\right)^{1/2}, \quad \text{or} \quad \frac{R}{A_0} \sim \gamma \left(\frac{A_0}{h_0}\right)^{-1/2}. \tag{64}$$

Hughes did not involve Carrier and Greenspan's solution to represent non-breaking waves, although this seems to be the obvious theoretical approach, at least as long as we are inside the shallow water regime. We notice that while (63) depends entirely on ξ, and (64) depends entirely on A_0/h_0, our expression (57) based on Carrier and Greenspan's theory depends on *both*. For irregular waves we therefore simply generalize (57) and (59)

$$\frac{R_{0.02}}{H_{m0}} = \left(\frac{1.6}{2}\right) 2\pi^{3/4} \left(\frac{H_{m0}}{2h_0}\right)^{-1/4} \xi^{-1/2}, \tag{65}$$

$$\frac{R_{0.02}}{H_{m0}} \le \left(\frac{1.6}{2}\right) \frac{1}{\pi} \xi^2. \tag{66}$$

Fig. 7 shows the experimental run-up data of Ahrens (1981). These data cover wave height to water depth ratios at the foot of the slope in the interval $0.09 \le H_{m0}/h_0 \le 0.30$, and consequently we plot (65) for $H_{m0}/h_0 = 0.09$ and 0.30. We realize that this is probably stretching the theory to the limit as wave conditions at the toe of the slope can hardly be considered linear as assumed in Sections 2 and 3. Nevertheless, the band covered by these two curves shown as (a) and (b) in Fig. 7 actually capture most

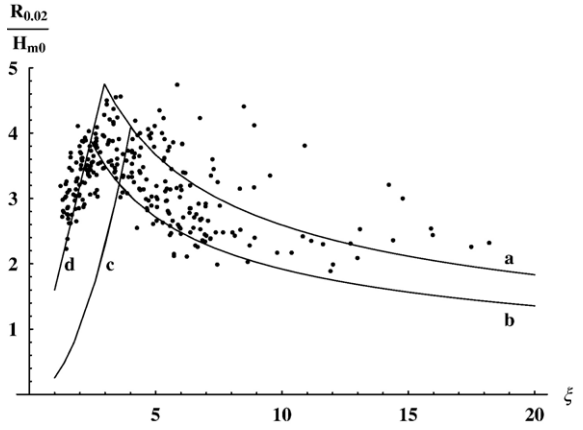

Fig. 7. Irregular wave run-up on smooth, impermeable slopes. Data from Ahrens (1981). a: (65) with $H_{m0}/h_0=0.09$; b: (65) with $H_{m0}/h_0=0.30$; c: Theoretical breaking criterium $0.8\xi^2/\pi$; d: Empirical breaking criterium 1.6ξ.

of the non-breaking events in Ahrens data, although there is admittedly still a certain scatter above this band. This is probably not surprising as wave–wave interactions such as short waves riding on long waves are not captured by the monochromatic theory. It is, however, quite clear that the theoretical saturated breaking curve shown as (c) in Fig. 7 is too restrictive, and that the empirical breaking curve (62) shown as (d) is in much better agreement with the data. As discussed in Section 3.4, Synolakis (1987) made a similar conclusion in connection with the run-up of solitary waves, where he observed that waves which were predicted to break according to the collapse of the Jacobian, actually did not break in reality. We therefore continue curves (a) and (b) until they reach the empirical breaking criterion (62) and find that a very large fraction of Ahrens data actually fall within this band of prediction. This suggests that (65) combined with (62) may provide a good estimate of the run-up of irregular waves. However, further investigations are necessary to confirm this conclusion.

7. Numerical results based on a high-order Boussinesq-type model

In this section, we present numerical simulations of non-linear wave run-up based on a recently extended highly accurate Boussinesq-type approach. The section serves the following purposes: We investigate what it takes to model the simple canonical test cases described in Sections 2–3, and we check if the numerical Boussinesq results agree with the theoretical expressions derived from the non-linear shallow water equations. In conclusion, we find special requirements on grid-size and time-step resolutions, and surprisingly good agreement between theory and modelling. Obviously, the capacity and the potential of the numerical model goes far beyond the canonical test cases presented here, but more advanced studies of e.g. landslide and earthquake generated waves are beyond the present scope of work and will be published later.

7.1. A brief summary of the method

The formulation was originally derived by Madsen et al. (2002, 2003) under a mild slope assumption, and has recently been extended to allow rapidly varying bathymetries (see Madsen et al., 2006), as well as moving wet–dry boundaries (see Fuhrman and Madsen, in press). The present method is based on Madsen et al. (2006) and solves the exact expressions for the kinematic and dynamic free surface conditions in terms of the surface elevation η, the horizontal surface velocity vector $\tilde{u}$ and the vertical surface velocity $\tilde{w}$. The Boussinesq-type formulation satisfies the Laplace equation by a velocity field expressed as a truncated series expansion enhanced with Padé techniques, involving up to fifth derivative operators. The expansion level $\hat{z}$ for the velocity field is restricted to vary slowly in space while there is no limitation on the spatial variation of the water depth. Throughout this work $\hat{z}$ is chosen to be mid-depth, $\hat{z}=-h/2$, except where the bottom exceeds the still water level $z=0$, where $\hat{z}=-h$.

Analysis and applications of the current method have shown that it retains highly accurate linear and non-linear properties for (wave number times depth) $kh\le 25$, provides accurate shoaling for $kh\le 30$, and gives accurate velocity kinematics for $kh\le 12$ (see e.g. Madsen et al., 2002, 2003, 2006, and Madsen and Agnon, 2003). Hence, over a large range of water depths this system may be considered as a highly accurate approximation of the exact Laplace problem governing non-linear water waves. As such, depth limitations conventionally associated with Boussinesq-type approaches are effectively eliminated by the present method for most practical applications. For details concerning the numerical method see Fuhrman and Bingham (2004), for various deep-water applications see Fuhrman et al. (2004) and Fuhrman and Madsen (2006), and for applications with rapidly varying bathymetries see Madsen et al. (2006).

The most recent model development is the implementation of a moving shoreline as described in detail by Fuhrman and Madsen (in press). This is based on the so-called "extrapolating boundary" method, which has previously been used by e.g. Lynett et al. (2002). The method begins by finding the last grid point where the total water depth $d=h+\eta$ exceeds some threshold δ, which is assumed small. Computed values at dry points (i.e. where $d<\delta$) are then replaced with those from a linear extrapolation based on the last two wet points. The algorithm is applied within the present model after each time-stepping stage evaluation. Testing has indicated that the results are not very sensitive to the chosen value of δ, and throughout the present work we use $\delta=R/200$, where R is the estimated run-up elevation from (57).

7.2. Numerical simulation of tsunami run-up

We will now use the numerical model to simulate non-linear wave run-up on a sloping beach. The model domain is constructed by connecting a flat region of depth h_0 to a sloping region with constant slope γ. One set of simulations is made with a sharp transition (Case A) and another set with a smoothed transition, which we find is a better representation of the infinite

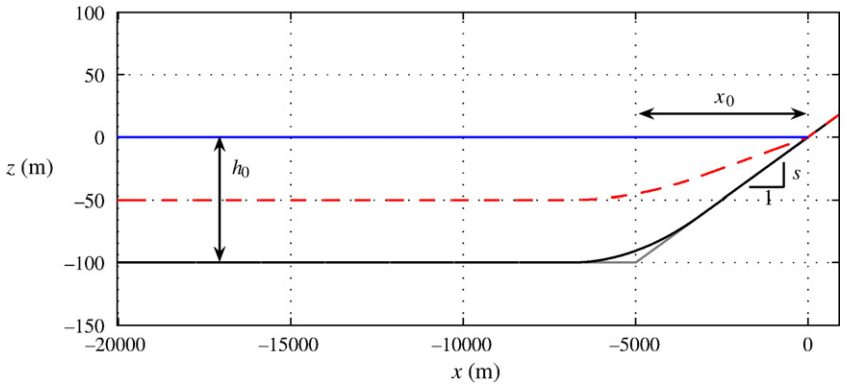

Fig. 8. Sketch of model bathymetries for Case A and Case B. The bold line indicates the sea bottom $-h(x)$ with a sharp transition from horizontal to sloping bottom (Case A). The dashed line indicates Case B with a smoothed transition. The dash-dotted line indicates the variation of $\hat{z}$.

slope problem (Case B), as the effects of the abrupt transition (but not the finite slope length) are removed. These cases are illustrated in the sample bathymetry provided in Fig. 8. The origin $(x, z)=0$ is here defined as the crossing of the sloping region and the still water level, with incoming waves at depth h_0 (and having wave length L_0, which should not be confused with the deep-water wave length $L_\infty=gT^2/2/\pi$) traveling in the $+x$-direction. The flat region (prior to any smoothing in Case B) has total length $2L_0$. The left-most $L_0/2$ consists of a relaxation zone used for the analytical wave generation. This is followed by an additional relaxation zone of equivalent length, where the analytical wave signal is gradually relaxed to the computed solution, which absorbs the wave field reflected off the slope. This leaves roughly one wave length for the generated wave to propagate freely before encountering the toe of the slope. We consider incoming periodic waves (based on linear wave theory) with $h_0=100$ m, slope $\gamma=1/50$ and with $A_0/h_0=0.01$, 0.005, 0.002 and 0.001, thus covering an order of magnitude in non-linearity. The wave period T is varied so that the surf-similarity parameter ξ generally covers the interval from roughly 6 to 20 in unit increments. The simulations are run for a sufficient length of time to essentially reach a repeating periodic state. We also note that in all cases dispersive terms incorporated in the Boussinesq-type formulation remain small, hence it is reasonable to compare against the non-dispersive theories discussed in Sections 2 and 3.

Most of the cases considered are discretized such that $R/\gamma/\Delta x=10$, where R is estimated from (57), which gives a constant spatial discretization of the run-up region, with the time step varied based on the Courant number constraint $Cr=c_0\Delta t/\Delta x=2$, where $c_0=L_0/T$ is the incident wave celerity. However, we have found that this discretization can lead to inaccurate results when the waves during the draw-down are near their breaking limits. To better maintain equivalent discretizations of the run-up and draw-down process in these more challenging cases, we introduce the notion of a *run-up Courant number* defined by

$$Cr_r = \frac{\Delta t}{T}\frac{4R}{\gamma \Delta x}, \tag{67}$$

which relates the temporal resolution of a wave period to the horizontal resolution of the moving shoreline, with a value of unity implying equivalent resolution (note that over one period, the moving shoreline covers a total horizontal distance $4R/\gamma$). This parameter is related to the conventional Courant number via

$$Cr_r = \left(\frac{4R}{\gamma L_0}\right) Cr, \tag{68}$$

hence by fixing Cr, the run-up Courant number C_{r_r} is inevitably varied, leading to values as low as $C_{r_r}\approx 0.02$ in the cases considered. When the waves are far from breaking (large ξ) this is not problematic, and we find that the results are not sensitive to these variations in C_{r_r}. However, in nearly breaking cases (low ξ) we have found significant sensitivity to this parameter, with small values of C_{r_r} resulting in significantly different run-up and (negative) draw-down elevations, which should theoretically be equivalent. In some cases (where $C_{r_r}<0.1$) a significant reduction in both has been observed, hence these inaccuracies seem to be related to dissipation introduced by the (first-order) extrapolations inherent within the run-up algorithm (see Lynett et al. 2002). For these reasons, the three cases considered nearest breaking (those with lowest ξ) for a given A_0/h_0 are discretized with an improved spatial resolution $R/\gamma/\Delta x=40$, and with the time step chosen such that $C_{r_r}=0.5$, which we find typically leads to very high accuracy, as will be demonstrated.

It should be stressed that in Case B, there are still obviously differences between our numerical setup, which is based on a flat bottom connected to a sloping region (which is then smoothed), and the analytical solution for an infinite plane slope. We find that reasonable agreement can be obtained when the slope length x_0 covers more than a quarter of the wave length L_0 which according to (30) and (56) yields

$$\frac{x_0}{L_0}>\frac{1}{4} \;\Rightarrow\; \sigma_0>\pi \;\Rightarrow\; \xi<\frac{2}{\sqrt{\pi}}\left(\frac{A_0}{h_0}\right)^{-1/2}.$$

In Case B, we restrict our comparison to within this range of the surf-similarity parameter.

Fig. 9a shows the computed envelope (comprised of spatial variations during a wave period) of the surface elevation for Case B with $A_0/h_0=0.005$ and $\xi=6$. Fig. 9b shows the corresponding envelope of the horizontal velocity, here simply taken as the velocity variable at $z=\hat{z}$, since the vertical

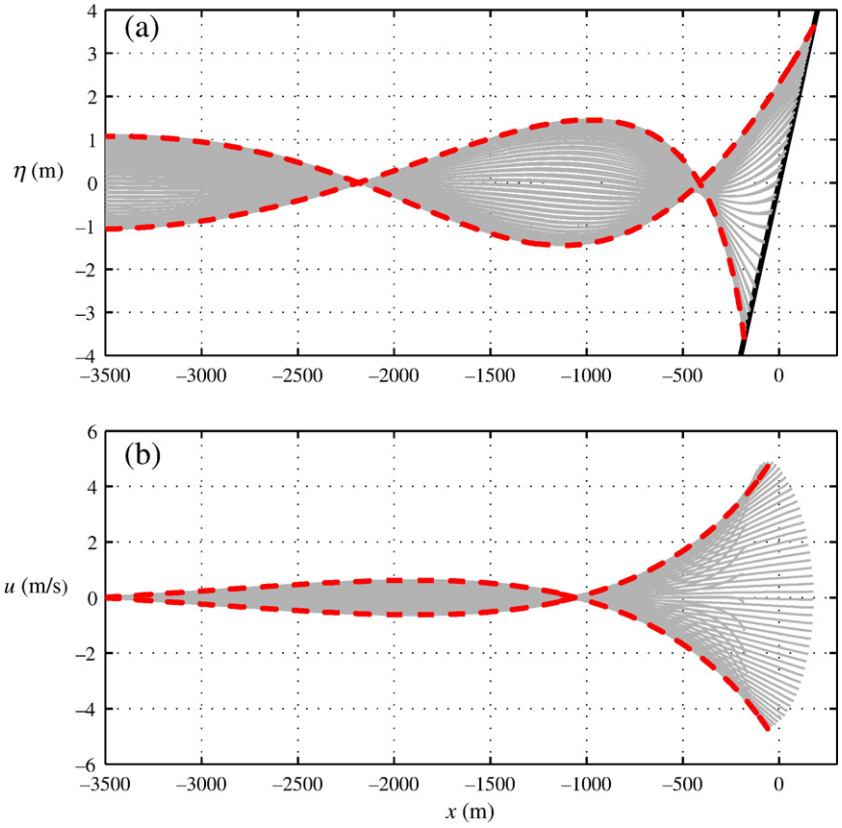

Fig. 9. Run-up envelopes showing (a) the surface elevation and (b) the associated velocities. Computed (thin grey lines) versus analytical theory by Carrier and Greenspan (1958) (bold dashed lines). Case: $T=240.1$ s, $A_0=0.5$ m, $h_0=100$ m (i.e. $\xi=6.0$, $A_0/h_0=0.005$).

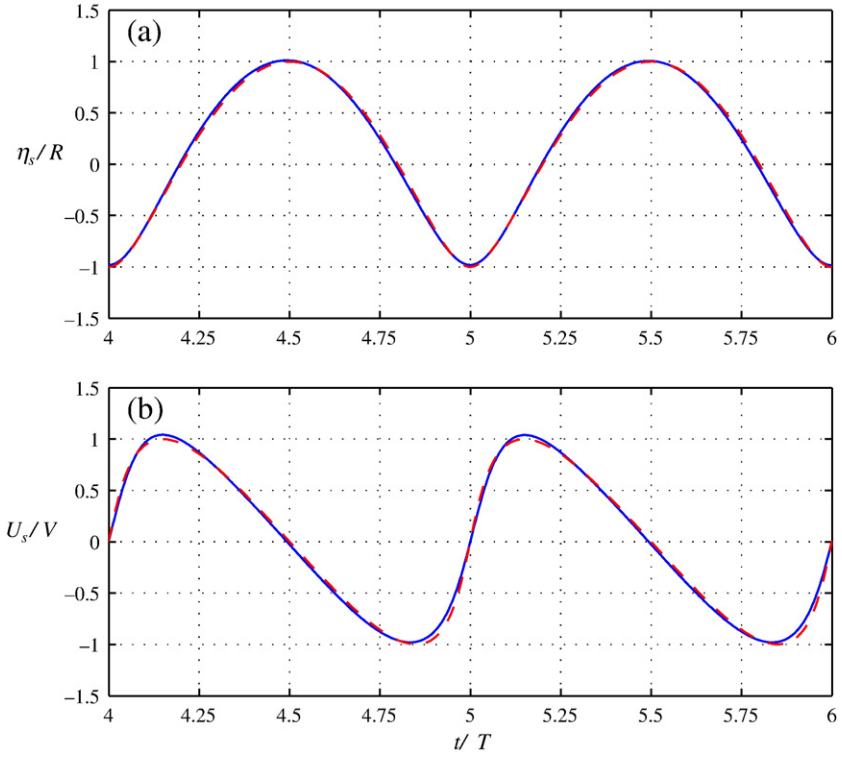

Fig. 10. Temporal variation of the non-linear shoreline motion showing the surface elevation (a) and the associated velocity (b). Full line: Theoretical solution given by (51). Dashed line: Numerical solution. Case: $T=240.1$ s, $A_0=0.5$ m, $h_0=100$ m (i.e. $\xi=6.0$, $A_0/h_0=0.005$).

distribution of the velocity field is nearly uniform. Time series of the shoreline elevation and shoreline velocity are also provided in Fig. 10. As expected, the velocity is close to its maxima near the still water shoreline ($x=0$), while it vanishes at maximum run-up and draw-down. The computed results are seen to be in very good agreement with the theoretical solution determined from (45)–(41).

Fig. 11 (Case A) and Fig. 12 (Case B) compare the computed and theoretical run-up elevations velocities as a function of ξ for the four different values of A_0/h_0. For comparative purposes, the filled circles in these figures represent the average of the computed maxima and (negative) minima (for elevations as well as velocities). To illustrate the previously described numerical inaccuracies which can occur at small ξ, the range of the computed maximum and minimum values are also provided (shown as error bars) for the cases with $A_0/h_0=0.005$. For most of the curves, these differences are actually negligible, and the error bars lie beneath the corresponding dots. The case with $\xi=8$ begins to show a more noticeable deviation, though this is obviously corrected in the three points to the left, which again use an improved spatial resolution and fixed run-up Courant number. Based on these results, Fig. 11 reveals an excellent agreement with the theoretical finite slope solution

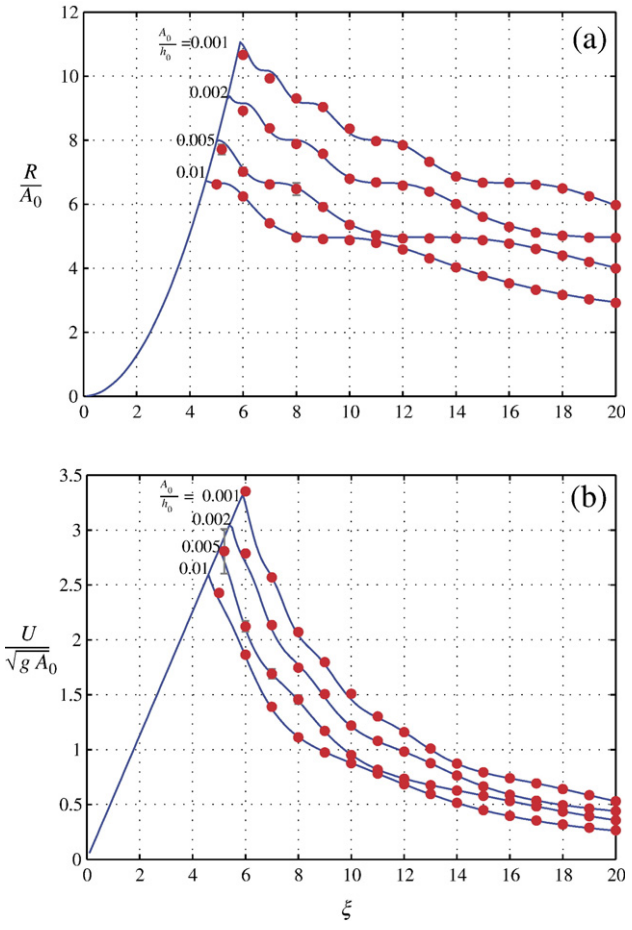

Fig. 11. Maximum non-dimensional run-up elevation (a) and the associated velocity (b) as a function of the surf-similarity parameter ξ. Filled circles are computed values using Case A with a sharp transition. Full lines are determined by the finite slope solution i.e. (29) with (56) for R and (58) for V.

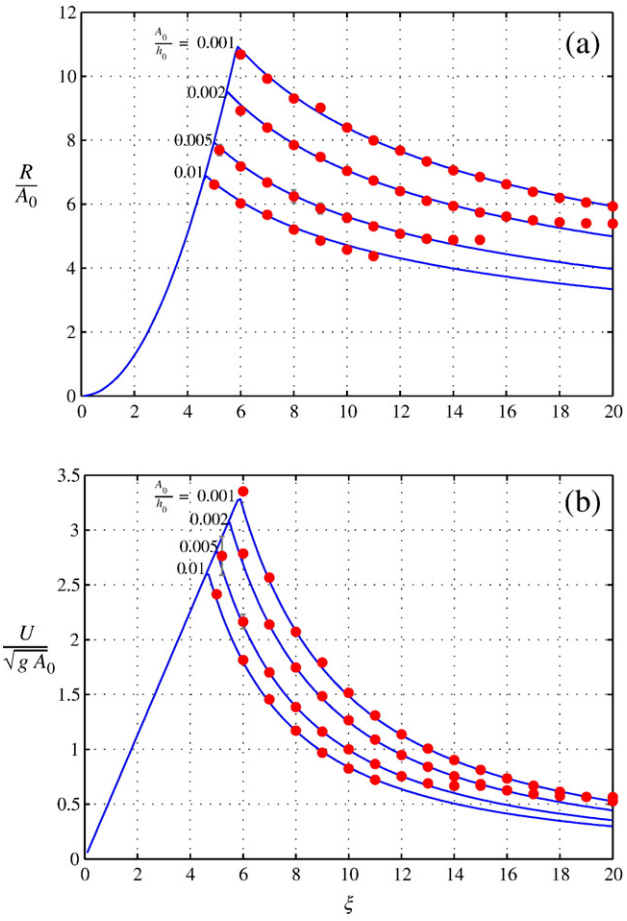

Fig. 12. Maximum non-dimensional run-up elevation (a) and the associated velocity (b) as a function of the surf-similarity parameter ξ. Filled circles are computed values using Case B with a smoothed transition. Full lines are determined by the infinite slope solution i.e. (57) for R and (58) for V.

determined by (29) with (56) for R, and (58) for V for the full range of parameters tested. The weakly oscillating behaviour of the solutions is faithfully captured by the numerical model. Somewhat more surprisingly, we also achieve an excellent agreement in Fig. 12 between the numerical results obtained with the smoothed transition for Case B and the theoretical infinite slope solution defined by (57) for R and (58) for V. As can be seen from these figures, we have managed to accurately compute cases up to the theoretical breaking limit (59). The close match obtained provides confidence in both the analytical solutions developed previously, as well as in the ability of the present numerical model to simulate this phenomenon over a wide range of parameter space.

8. Conclusions

In this work we have reviewed and re-examined the classical solutions by Green (1838), Lamb (1932), Keller and Keller (1964) and Carrier and Greenspan (1958) for the run-up of periodic long waves on a sloping beach. Section 2 covers the linear problem of run-up on an infinitely long constant slope and on a finite constant slope connected to an offshore flat region. The difference between the two solutions is shown to be

small. Section 3 covers the non-linear run-up solution. While the maximum run-up/rundown elevations and velocities are identical to the corresponding linear solutions established in Section 2, the temporal and spatial variation of the non-linear solution is quite different from the linear one, and it provides a theoretical breaking criterion corresponding to the collapse of the non-linear coordinate transformation.

In Section 4, we introduce the surf-similarity parameter and quantify the maximum run-up and the associated flow velocity in terms of this parameter and the amplitude to depth ratio determined at some offshore location. As a first approximation, these solutions are combined with the theoretical breaking criterion under the assumption of a saturated breaking process. These theoretical expressions provide an easy first assessment of the impact on a given beach by a tsunami with a certain approximate wave period and wave height at an initial depth. In Section 5, we conclude that it is the combination of huge run-up elevations and extreme run-up velocities, which makes a tsunami such a devastating event compared to other types of wave events such as tides and wind waves. We also conclude that the destructive effects depend very much on the beach slope versus the incoming wave steepness i.e. the surf-similarity parameter, and this explains why some beaches were hit so much worse than their neighbours during the recent Indian Ocean tsunami on December 26, 2004. Measurements were collected off the coastline of Phuket, Thailand indicating a typical wave period of 13 min and a typical wave height of 5 m in 14 m water depth. On the basis of this information combined with the analytical expressions from Section 5, we conclude that the impact on flat beaches with slopes of the order 1/100 is huge compared to the impact on steep beaches with slopes of the order 1/15. Qualitatively this analysis explains the observations from Thailand, where the flat Kamala beach was completely destroyed, while the neighbouring steep Surin beach was left almost untouched.

In Section 6 we address the problem of run-up of irregular wind waves on steep impermeable slopes. A recent review made by Hughes (2004) has revealed that existing empirical expressions for the run-up of non-breaking regular and irregular waves are quite inadequate to capture the observed scatter. Hughes therefore concluded that the surf-similarity parameter was probably not a good choice as the governing parameter for the run-up. Given the demonstrated theoretical dependance for regular long waves, we tend not to agree with this conclusion and suggest to replace the empirical curve fits for non-breaking waves with Carrier and Greenspan's shallow water theory from Section 4. According to this theory a moderate, but predictable, scatter will indeed occur simply because of the different wave height to water depth ratios. We adjust the theory for irregular wave statistics and compare the theoretical curves to the data by Ahrens (1981). A fairly good agreement with non-breaking wave events is achieved, while it is concluded that Carrier and Greenspan's theoretical breaking criterion is too restrictive compared to the measurements. It is suggested that this criterion be replaced by Hunt's (1959) criterion for breaking waves.

Finally, in Section 7, we present numerical run-up results obtained by running a high-order Boussinesq-type model. The model is based on a formulation, which was originally derived by Madsen et al. (2002, 2003) for slowly varying bathymetries, but which has recently been extended to rapidly varying bathymetries (Madsen et al., 2006) and moving wet/dry shorelines (Fuhrman and Madsen, in press). The formulation allows for dispersive non-linear wave motion, but here we restrict applications to the run-up of long waves and compare the results to the shallow water expressions obtained in Sections 2–4. The agreement with the infinite slope as well as with the finite slope expressions is excellent except that the numerical model predicts a (usually minor) discrepancy between run-up and draw-down which is absent in the theoretical solutions.

Acknowledgements

Special thanks to Dr. Steven A. Hughes, who provided the experimental results for run-up of regular and irregular waves on digital form. Also thanks to Mr Thomas Siffer, who provided Fig. 5 and the information concerning the circumstances of the recording. Finally, we sincerely thank the Danish Technical Research Council, who financed this work (STVF Grant no. 9801635), as well as the Danish Center for Scientific Computing for providing computational resources.

References

Ahrens, J.P., 1981. Irregular wave runup on smooth slope. CETA No. 81-17. U.S. Army Corps of Engineers, Coastal Engineering Research Center, FT. Belvoir, VA.

Ammon, C.J., et al., 2005. Rupture process of the 2004 Sumatra–Andaman earthquake. Science 308, 1133–1339.

Arcas, D., Titov, V., 2006. Sumatra tsunami: lessons from modelling. Surv. Geophys. 27, 679–705.

Bagai, D.S., et al., 2005. Tsunami Thailand one year after international response and contribution of international partners. United Nations Development Programme report. 120 pp., www.undp.or.th/publications/index.html.

Battjes, J.A., 1974. Surf similarity. Proc. 14th Int. Coastal Eng. Conf., vol. 1. ASCE, pp. 466–480.

Bilham, R., 2005. A flying start, then a slow slip. Science 308, 1126–1127.

Borrero, J.C., 2005. Field data and satellite Imagery of tsunami effects in Banda Aceh. Science 308 (5728), 1596.

Borrero, J.C., Sieh, K., Chlieh, M., Synolakis, C.E., 2006. Tsunami inundation modelling for western Sumatra. PNAS 103 (52), 19673–19677.

Bowman, F., 1958. Introduction to Bessel functions. Dover Publications Inc., New York. 135 pp.

Burcharth, H.F., Hughes, S.A., 2002. Fundamentals of design. In: Hughes, S. (Ed.), Coastal Engineering Manual, Part VI, Design of Coastal Project Elements, Chapter VI-5, Engineer Manual 1110-2-1100. Army Corps of Engineers, Washington DC.

Carrier, G.F., Greenspan, H.P., 1958. Water waves of finite amplitude on a sloping beach. J. Fluid Mech. 4, 97–109.

Carrier, G.F., Wu, T.T., Yeh, H., 2003. Tsunami runup and drawdown on a plane beach. J. Fluid Mech. 475, 79–99.

Fuhrman, D.R., Bingham, H.B., 2004. Numerical solutions of fully nonlinear and highly dispersive Boussinesq equations in two horizontal dimensions. Int. J. Numer. Methods Fluids 44, 231–255.

Fuhrman, D.R., Madsen, P.A., 2006. Short-crested waves in deep water: a numerical investigation of recent laboratory experiments. J. Fluid Mech. 559, 391–411.

Fuhrman, D.R., Madsen, P.A., in press. Simulation of nonlinear wave run-up with a high-order Boussinesq model. Coast. Eng.

Fuhrman, D.R., Madsen, P.A., Bingham, H.B., 2004. A numerical study of crescent waves. J. Fluid Mech. 513, 309–341.

Fujii, Y., Satake, K., 2007. Tsunami source of the 2004 Sumatra–Andaman earthquake inferred from tide gauge and satellite data. Bull. Seismol. Soc. Am. 97 (1A), 192.

Galvin, C.J., 1968. Breaker type classification on three laboratory beaches. J. Geophys. Res. 73, 3651–3659.

Geist, E.L., Bilek, S.L., Arcas, D., Titov, V.V., 2006. Differences in tsunami generation between the December 26, 2004 and March 28, 2005 Sumatra earthquakes. Earth Planets Space 58, 185–193.

Gjevik, B., Pedersen, G., 1981. Run-up of long waves on an inclined plane. Preprint Series Inst. of Math. Univ. of Oslo. ISBN: 82-553-0453-3. 25 pp.

Gower, J., 2005. Jason 1 detects the 26 December 2004 tsunami, Eos Trans. AGU 86 (4), 37.

Granthem, K.N., 1953. A model study of wave run-up on sloping structures. Technical report, vol. 3. Institute of Engineering Research, University of California, Berkeley, California. Issue 348.

Green, G., 1838. On the motion of waves in a variable canal of small depth and width. Trans. Camp. Philos. Soc. 6, 457–462.

Grilli, S.T., Ioualalen, M., Asavanant, J., Shi, F., Kirby, J.T. and Watts, P. (2007) Source constraints and model simulation of the December 26, 200 Indian Ocean Tsunami, In Press for J. Waterways, Port, Ocean and Coastal Engineering.

Harada, K., 2005. The December 26, 2004 Sumatra earthquake tsunami, tsunami field survey around Phuket, Thailand. Report from Kyoto University, Japan. www.drs.dpri.kyoto-u.ac.jp/sumatra/thailand/phuket_survey_e.html.

Hughes, S.A., 2004. Estimation of wave run-up on smooth, impermeable slopes using the wave momentum flux parameter. Coast. Eng. 51, 1085–1104.

Hunt, I.A., 1959. Design of seawalls and breakwaters. J. Waterw. Harb. Div., ASCE 85 (WW3), 123–152.

Ioualalen, M., Asavanant, J., Kaewbanjak, N., Grilli, S.T., Kirby, J.T. and Watts, P. (2007) Modelling the 26th December 2004 Indian Ocean tsunami: Case study of impact in Thailand. In Press for J. Geophysical Research.

Iribarren, C.R., Nogales, C., 1949. Protection des Ports. XVIIth International Navigation Congress, Section II, Communication, pp. 31–80.

Keller, J.B., Keller, H.B., 1964. Water wave run-up on a beach. ONR Research Rep. Contract NONR-3828(00). Depth. of the Navy, Washington, D.C. 40 pp.

Lamb, H., 1932. Hydrodynamics. Cambridge University Press.

Lynett, P., Liu, P.L.-F., 2002. A numerical study of submarine-landslide-generated waves and run-up. Proc. R. Soc. Lond. A. 458, 2885–2910.

Madsen, P.A., Agnon, Y., 2003. Accuracy and convergence of velocity formulations for water waves in the framework of Boussinesq theory. J. Fluid Mech. 477, 285–319.

Madsen, P.A., Bingham, H.B., Liu, H., 2002. A new Boussinesq method for fully nonlinear waves from shallow to deep water. J. Fluid Mech. 462, 1–30.

Madsen, P.A., Bingham, H.B., Schäffer, H.A., 2003. Boussinesq-type formulations for fully nonlinear waves and extremely dispersive water waves: derivation and analysis. Proc. R. Soc. Lond., A 459, 1075–1104.

Madsen, P.A., Simonsen, H.J., Pan, C.-H., 2005. Numerical simulation of tidal bores and hydraulic jumps. Coast. Eng. 52, 409–433.

Madsen, P.A., Fuhrman, D.R., Wang, B., 2006. A Boussinesq-type method for fully nonlinear waves interacting with a rapidly varying bathymetry. Coast. Eng. 53, 487–504.

Mei, C.C., 1989. The applied dynamics of ocean surface waves. World Scientific. 740 pp.

Mei, C.C., Stiassnie, M., Yue, D.K.-P., 2005. Theory and applications of ocean surface waves. Advanced Series on Ocean Engineering, vol. 23. World Scientific, Singapore.

Saville Jr., T., 1956. Wave run-up on shore structures. J. Waterw. Div. 82 (WW2), 925(1)–925(14).

Synolakis, C.E., 1987. The runup of solitary waves. J. Fluid Mech. 185, 523–545.

Titov, V., Rabinovich, A.B., Mofjeld, H.O., Thomson, R.E., Gonzalez, F.I., 2005. The global reach of the 26 December 2004 Sumatra tsunami. Science 309, 2045–2048.

Wang, X., Liu, P.L.-F., 2006. An analysis of 2004 Sumatra earthquake fault plane mechanisms and Indian Ocean tsunami. J. Hydraul. Res. 44 (2), 147–154.